Iranian Journal of Astronomy and Astrophysics
Vol. 6, No. 1, Spring 2019
©Available online at http://journals.du.ac.ir
DOI:10.22128/ijaa.2019.343.1056

Iranian Journal of Astronomy and Astrophysics

Different Magnetic Field Distributions in Deformed Neutron Stars

Mina Zamani[1] · Mohsen Bigdeli[2]

[1] Department of Physics, University of Zanjan, P.O. Box 45195-313, Zanjan, Iran
[2] Department of Physics, University of Zanjan, P.O. Box 45195-313, Zanjan, Iran

Abstract. In this work, we review the formalism which would allow us to model magnetically deformed neutron stars. We study the effect of different magnetic field configurations on the equation of state (EoS) and the structure of such stars. For this aim, the EoS of magnetars is acquired by using the lowest order constraint variational (LOCV) method and employing the AV_{18} potential. We show how the magnetic field varies from the surface to the center of neutron star by using various exponential and polynomial profiles and compare their results. In addition, global properties of neutron stars are obtained within two formalisms. The first formalism is described by considering the pressure into two directions and the deformation of neutron stars is governed by anisotropies in the equation of state. The second formalism for investigating macroscopic properties of magnetars is gained by treating the nonuniform pressure as a perturbation to the total pressure and expanding metric and pressure up to the quadrupole term in spherical harmonics. Afterwards, we include three nucleon interactions (TNI) to the EoS and apply this model to represent our results for both exponential and polynomial magnetic field profiles. The maximum gravitational mass is obtained in the range of (1.71-1.80) $M_\odot$ and (2.13-2.19) $M_\odot$ for the EoS without and with TNI contribution, respectively.

Keywords: magnetars, magnetic field profiles, deformed neutron stars

1 Introduction

There is a growing interest in new classes of young neutron stars known as magnetars [1, 2], namely, the anomalous X-ray pulsars, the soft γ-ray repeaters and more recently, the repeating fast radio burst [3]. Observational data indicate that the magnetic field on the surface of magnetars can be as strong as $10^{14} - 10^{15}$ G, which is three orders of magnitude larger than the one in standard neutron stars. While such observations only constrain the surface magnetic field, there is no way to measure the internal magnetic field. Moreover, due to the scalar Virial theorem, the magnetic field in the core of magnetars can reach values larger than 10^{18} G [4]. Despite the great theoretical effort of the last forty years, the exact mechanism to generate such high magnetic field is yet to be known but the first hypothesis is that the fields may be inherited from the progenitor star and amplified during the gravitational collapse due to the magnetic flux conservation [5]. Another hypothesis is that the plasma of a protoneutron star rotates rapidly and the magnetic field amplifies. The magnetohydrodynamic (MHD) dynamo mechanism is the most accepted theory to define the magnetic field of the magnetars [1]. Current information of 29 magnetars is available in magnetar catalog and it is estimated that magnetars constitute approximately 10% of neutron star population [6, 7].

After the discovery of magnetars, a large amount of research has been done on the issue of how magnetic fields modify the microscopic structure (represented in the equation of state) and the macroscopic structure (obtained from the solution of Einstein-Maxwell equations) of neutron stars [8, 9, 10, 11, 12, 13, 14, 15, 16, 17, 18]. In order to include the effects of magnetic field on the EoS, a profile for the strength of the field has to be defined. Since, there is no information directly available on the interior magnetic field of the neutron star, different configurations have been employed to simulate the variation of the field. Many authors [11, 14, 19, 20] employed an exponential baryon number density-dependent parameterization which was proposed twenty years ago by Bandyopadhyay [21], where the magnetic field profile is given by,

$$B = B_s + B_c \left[1 - exp(-\beta(\frac{\rho}{\rho_0})^\gamma)\right] \tag{1}$$

with two free parameters β and γ. In this parameterization, B_s and B_c are the magnetic fields on the surface and the center of the neutron stars and ρ_0 is the nuclear saturation density.

Moreover, with the purpose of reducing the number of free parameters from two to one, Lopes and Menezes [22] proposed another profile, which depends on the energy density rather than on the baryon number density,

$$B = B_s + B_c(\frac{\varepsilon_M}{\varepsilon_c})^\gamma \tag{2}$$

where ε_c is the central energy density of the maximum mass nonmagnetized neutron star, ε_M is the energy density of the matter alone and γ is any positive number.

In addition, Dexheimer *et al.* introduced a variable magnetic field as a function of the baryon chemical potential [23],

$$B = B_s + B_c \left[1 - \exp(b\frac{(\mu_B - 938)^a}{938})\right] \tag{3}$$

with $a = 2.5$, $b = 4.08 \times 10^{-4}$ and μ_B given in MeV. This profile avoids a phase transition induces a discontinuity in the effective magnetic field.

The primary challenge for simulating the magnetic field profiles is maintaining the divergence-free constraint of the field. However, as already pointed out by Menezes and Alloy [24], such ad hoc exponential formulations for magnetic field profiles do not fulfill the "no-monopoles" constraint. Therefore, Dexheimer *et al.* suggested that magnetic fields increase slowly with increasing baryon chemical potential of magnetized matter. More precisely, they declared that the increase is polynomial instead of exponential and the shape of the profile is well fit by a quadratic polynomial [25],

$$B = \frac{(a + b\mu_B + c\mu_B^2)}{(B_c^e)^2}\mu \tag{4}$$

where a, b, c are coefficients determined from the numerical fit, μ is the dipole magnetic moment and $B_c^e = 4.414 \times 10^{13}$ G is the electron critical field.

Recently, Chatterjee *et al.* [26] proposed a "universal" eighth-order polynomial fit for the magnetic field profile as a function of stellar radius, obtained from a full numerical calculation of the magnetic field distribution,

$$B = B_c \times (1 - 1.6x^2 - x^4 + 4.2x^6 - 2.4x^8) \tag{5}$$

where $x = \frac{r}{r_{mean}}$ is the ratio between the radius r in Schwarzschild coordinates and the stars mean radius.

In order to develop a formalism that describes magnetars in general relativity framework, it is necessary to solve the coupled Einstein-Maxwell equations. The equilibrium of spherically symmetric, nonrotating neutron stars is governed by the TOV equations, that follow from the Einstein equations with an isotropic energy-momentum tensor of the form: $\mathrm{diag}(\varepsilon, p, p, p)$. However, the energy-momentum tensor of the magnetic field is anisotropic: $\mathrm{diag}(\frac{B^2}{8\pi}, \frac{B^2}{8\pi}\frac{B^2}{8\pi}, -\frac{B^2}{8\pi})$ and the TOV equations are not valid for this situation. Anisotropy of magnetic pressure causes deformations in neutron stars; hence, the stellar macroscopic structure needs a general two-dimensional (2D) treatment. The multipole deformation of magnetized Newtonian stars was investigated by Chandrasekhar & Fermi [27] and Ferraro [28]. The fully general relativistic approach was developed numerically by Bonazzola *et al.* [29] and was applied by Bocquet *et al.* [30] and Cardall *et al.* [31], to investigate the effects of magnetic field on the structure of neutron stars. They solved general relativistic equations exactly for a dipolar magnetic field. This formalism was applied for either poloidal [30, 32, 33] or toroidal [34, 35] magnetic fields and was employed to describe quark stars [36], hybrid stars [17] and hyperon matter [18]. An analytic and semianalytic solutions for the deformation of the magnetars were proposed by many authors [32, 37, 38, 39, 40, 41], where the perturbation of the metric was carried out.

In this work, we employ three different magnetic field profiles and study the effects of these various configurations on the EoS and structure of neutron stars. We find out the EoS of magnetized neutron matter using the lowest-order constraint variational (LOCV) method [42] without and with TNI [43] contribution. In addition, the influences of different magnetic field configurations on the global properties of neutron stars are investigated within two perturbed metrics.

The plan of this paper is as follows. In Sect. 2, different magnetic field profiles is performed. In Sect. 3 we outline the formalism used to study the structure of deformed neutron stars. Additionally, the impact of various magnetic field configurations with different parameterization is found out on the gravitational mass and deformation of magnetars. Conclusions are summarized in Sect. 4.

2 Different magnetic field profiles

Since neither the analytical data nor the observational data contains information about the variation of the magnetic field in neutron star interior, three different field profiles are performed in this section and their results are compared. These profiles are proposed in the form of exponential baryon number density-dependent magnetic field (P1), energy density-dependent magnetic field (P2) and polynomial baryon number density-dependent magnetic field (P3),

$$\begin{aligned} P1 : B(\rho) &= \alpha B_c^e + \alpha \times 10^4 B_c^e \left[1 - exp(-\beta(\frac{\rho}{\rho_0})^\gamma)\right] \\ P2 : B(\varepsilon) &= \alpha B_c^e + \alpha \times 10^4 B_c^e (\frac{\varepsilon_M}{\varepsilon_c})^\gamma \\ P3 : B(\rho) &= 10^4 B_c^e (1 + \alpha \left[\beta(\frac{\rho}{\rho_0})^\gamma - \frac{1}{2}(\beta)^2(\frac{\rho}{\rho_0})^{2\gamma}\right]) \end{aligned} \quad (6)$$

where $\varepsilon_c = 39.579 \times 10^{14} \frac{g}{cm^3}$ and $\alpha = 5$ is the field intensity. In this literature, we compare the results of different profiles by employing several sets of β and γ as arbitrary parameters.

In Fig. 1, we have plotted three configurations of magnetic field for different parameterization of β and γ. It is evident from the figure that although both P1 and P2 prescriptions have an exponential form, the P1 profile reaches the maximum value of the magnetic field in lower densities. We should notice that the magnetic field increase in the polynomial profile is significantly less than in the exponential ones. To describe this effect quantitatively, the corresponding magnitudes of the magnetic field in the surface and center of magnetars, are collected in Tab. 1.

The magnetic field in the radial direction can be obtained for the maximum mass configuration from the TOV solution where r runs from the center to the surface of the neutron star. The profiles are displayed as a function of the star's radius in Fig. 2.

3 Structural properties of magnetars

In this section, we review different formalisms normally used to describe the structure of magnetars and compare their results. For this purpose, we develop three different metrics that aim to define how magnetic field modify global properties of neutron stars.

The first formalism (M1) is obtained by considering spherically symmetric static distributions of matter which its line element is given by [44],

$$M1 : ds^2 = -e^{\nu(r)}dt^2 + e^{\lambda(r)}dr^2 + r^2(d\theta^2 + sin^2\theta d\phi^2) \tag{7}$$

where ν and λ are shown in the geometric unit ($c = G = 1$) by

$$\frac{d\nu}{dr} = -\frac{2}{\varepsilon_m + p_m}\frac{dp}{dr}, \tag{8}$$

$$e^{\lambda} = (1 - \frac{2m(r)}{r})^{-1}. \tag{9}$$

In these equations, the contribution of the electromagnetic field ($\frac{B^2}{8\pi}$) is directly summed to the energy density and pressure of the matter as,

$$\varepsilon = \varepsilon_m + \frac{B^2}{8\pi}, \quad p = p_m + \frac{B^2}{8\pi} \tag{10}$$

where the subscript m stands for the matter contribution of the EoS. For this solution, the magnetic field profile is added isotropically to the EoS, but the field contribution should enter with different signs in different directions in the energy-momentum tensor. Therefore, the TOV solution is not correct; however, this is a frequently used assumption in the literatures and the TOV results are mentioned only for comparison.

Moreover, it is important to notice that anisotropy in pressure, which breaks the spherical symmetry of the system results in two-dimensional treatment. To clarify more, we should define distinct pressure gradients in the polar and equatorial directions that cause deformation in the neutron stars. We introduce the perpendicular and parallel pressures with respect to the direction of magnetic field as $p_\perp = p_m + \frac{B^2}{8\pi}$ and $p_\parallel = p_m - \frac{B^2}{8\pi}$. In order to model deformation due to the a non-isotropic equation of state, one must have hydrostatic equilibrium equations both in the radial and polar directions. For this aim, the geometry of the system is descibed by the metric M2.

$$\begin{aligned} M2 : ds^2 &= -e^{2\lambda}dt^2 + e^{-2\lambda}[e^{2\nu}(dr^2 + dz^2) \\ &+ r^2 d\phi^2] \end{aligned} \tag{11}$$

Hence, the hydrostatic equilibrium equations modify to the four coupled sets of ordinary differential equations for our two dimensional parameterized model.

$$\frac{\partial p_{\parallel}}{\partial z} = -\frac{(\varepsilon + p_{\parallel})(\frac{z}{2} + 4\pi z^3 p_{\parallel} - \frac{z}{2}(1 - \frac{2M(r,z)}{z}))}{z^2(1 - \frac{2M(r,z)}{z})}, \tag{12}$$

$$\frac{\partial p_{\perp}}{\partial r} = -\frac{(\varepsilon + p_{\perp})(\frac{r}{2} + 4\pi r^3 p_{\perp} - \frac{r}{2}(1 - \frac{2M(r,z)}{r}))}{r^2(1 - \frac{2M(r,z)}{r})}, \tag{13}$$

$$\frac{dm_{\parallel}}{dz} = \frac{4}{3}\pi r^2 \varepsilon, \tag{14}$$

$$\frac{dm_{\perp}}{dr} = \frac{8}{3}\pi r z \varepsilon. \tag{15}$$

These equations are coupled together with the gravitational mass $M(r,z) = m_{\perp} + m_{\parallel}$. For more details see Ref. [41].

And finally the third formalism (M3) is obtained by formulating the general metric as a multipole expansion around spherically symmetric space-time [38] similar to the method developed by Hartle and Thorne [45, 46] for slowly rotating neutron stars.

$$\begin{aligned} M3 : ds^2 &= -e^{\nu(r)}\left\{1 + 2\left[h_0(r) + h_2(r)P_2(cos\theta)\right]\right\}dt^2 \\ &+ e^{\lambda(r)}\left\{1 + \frac{e^{\lambda(r)}}{r}\left[m_0(r) + m_2(r)P_2(cos\theta)\right]\right\}dr^2 \\ &+ r^2\left[1 + 2k_2(r)P_2(cos\theta)\right](d\theta^2 + sin^2\theta d\phi^2), \end{aligned} \tag{16}$$

where $P_2(cos\theta)$ is the Legendre polynomial of order 2 and h_0, h_2, m_0, m_2 and k_2 are second order corrections which correspond to deviation from spherical shape. The pressure p can also be expanded in multipoles as,

$$p = p_m + \left[p_0 + p_2 P_2(cos\theta)\right], \tag{17}$$

where $p_0 = \frac{1}{3}(\frac{B^2}{8\pi})$ is the monopole contribution and $p_2 = -\frac{4}{3}(\frac{B^2}{8\pi})$ is the quadrupole contribution of the magnetic pressure. From the Einstein equations, we can obtain unknown functions h_0, h_2, m_0, m_2 and k_2 [47].

The gravitational mass (M), the equatorial radius (R_e) and the polar radius (R_p) of the deformed magnetar can be determined by the following equations [45, 46],

$$M = M_0 + m_0, \tag{18}$$

$$R_e = R + \xi_0(R) - \frac{1}{2}\left[\xi_2(R) + Rk_2\right], \tag{19}$$

$$R_p = R + \xi_0(R) + \left[\xi_2(R) + Rk_2\right], \tag{20}$$

where M_0 is the mass for matter term and m_0 is an additional mass due to magnetic term; R is the radius of the spherical star and ξ_0 and ξ_2 are given by [45],

$$\xi_0(r) = \frac{r^2\left[1 - \frac{2m(r)}{r}\right]}{\left[4\pi r^3 p_m + m(r)\right]}h_0, \tag{21}$$

$$\xi_2(r) = \frac{r^2\left[1-\frac{2m(r)}{r}\right]}{[4\pi r^3 p_m + m(r)]}h_2. \tag{22}$$

In order to solve the hydrostatic equations and find out the mass-radius relation in neutron stars, we use the LOCV method for describing the EoS.

In the following, we briefly obtain the energy density of magnetized neutron matter using the LOCV method with the modern AV_{18} two-body potential. It is important to note that in this literature β-stable matter is approximated by the pure neutron matter. This approximation is also used in some other studies [47, 48, 49, 51, 52, 50]. The Helmholtz free energy, F [53] should be calculated in order to gain the magnetic properties, equilibrium state and the pressure, p_m, of the system at the external magnetic field,

$$\begin{aligned} F &= E - BM, \\ p_m &= \rho^2 \frac{\partial F}{\partial \rho}. \end{aligned} \tag{23}$$

in this equation, M is the magnetization given by,

$$M = \frac{1}{N}\int m dV, \qquad m = \mu_n \rho \delta, \tag{24}$$

where $\mu_n = -6.0307738 \times 10^{-18}$ MeV/G is the neutron magnetic moment, and E is the total energy per particle of spin polarized neutron matter calculated by the LOCV method. In this method, we consider a trial many-body wave function of the form $\psi = \mathcal{F}\phi$, in which ϕ is Slater determinant of the plane waves and $\mathcal{F} = \mathcal{F}(1\cdots N)$ is a proper N-body correlation operator which can be replaced by a Jastrow form i.e., $\mathcal{F} = \mathcal{S}\prod_{i>j} f(ij)$, where $\mathcal{S}$ is a symmetrizing operator. In addition, we consider the cluster expansion of the energy functional up to the two-body term [54],

$$E([f]) = \frac{1}{N}\frac{\langle\psi|H|\psi\rangle}{\langle\psi|\psi\rangle} = E_1 + E_2. \tag{25}$$

The smallness of the three-body cluster energy has been discussed in [42, 55], where it is shown that our cluster expansion converges reasonably and it is a good approximation to stop after the two-body energy term.

For the neutron matter, the one-body term E_1 is,

$$E_1 = \sum_{\sigma=\uparrow,\downarrow}\sum_{k\leq {k_F}^\sigma}\frac{\hbar^2 k^2}{2m_n}, \tag{26}$$

where ${k_F}^\sigma = (6\pi^2\rho^\sigma)^{1/3}$ is the Fermi momentum of each component of the system and m_n is the neutron mass. The two-body energy E_2 is,

$$E_2 = \frac{1}{2N}\sum_{ij}\langle ij\,|\nu(12)|\,ij-ji\rangle, \tag{27}$$

where

$$\nu(12) = -\frac{\hbar^2}{2m_n}[f(12),[\nabla_{12}^2, f(12)]] + f(12)V(12)f(12). \tag{28}$$

Here, $f(12)$ and $V(12)$ are the two-body correlation and potential. In our calculations, we have used the AV_{18} two-body potential. For more details of our calculations, see Refs. [56,

57, 58]. We have also added the contribution of TNI to AV_{18} two-body potential [59] and compare the microscopic and macroscopic properties of magnetars without and with inclusion of TNI contribution.

Fig. 3 shows the equation of state of neutron matter for different magnetic field configurations and different parameterization of β and γ without TNI contribution. For non-zero magnetic field the pressure splits into the parallel and perpendicular components, which are increasing functions of density. Moreover, for P2 and for $\gamma > 1$, we obtain a parameter free model.

We have summerized the global properties of magnetars for different magnetic field profiles and different approaches in Tab. 1. In this table, the parameters such as the values of magnetic field in the surface and center (B), the maximum gravitational mass (M), the equatorial radius (R_e) and the deformation constant ($\frac{R_p}{R_e}$) are shown for different sets of β and γ. It is clear that larger maximum mass is obtained by using P1 prescription for all metrics, while for P2 and $\gamma > 1$, all macroscopic properties are approximately the same. For P3 smaller values of deformation constant are obtained which indicates that the star gets more oblate. The parameters listed in this table is constained by the EoS without TNI contribution

We have displayed the mass-radius relation in Fig. 4 for three different hydrostatic equilibrium equations obtained from M1, M2 and M3 and for the EoS without TNI contribution. We have chosen one set of β and γ for each profile. Regarding to polynomial profile, the parallel pressure is negative up to densities about $(0.3 - 0.4)fm^{-3}$ because of strong magnetic field on the surface of the star. Therefore, the figure of polynomial profile for M3 is plotted for gravitational mass greater than $0.6M_{\odot}$.

Finally, the gravitational mass as a function of equatorial radius for the EoS including TNI, is plotted in Fig. 5. The EoS of neutron matter with TNI contribution is also merged in this figure. In this figure, we have chosen one set of β and γ for the third formalism (M3) and for the P1 and P3 profiles. We obtain maximum gravitational mass of $(2.17 - 2.18)M_{\odot}$ $[(2.13 - 2.19)M_{\odot}]$ for 2-dimensional (M3) [TOV (M1)] solutions. An analogous analysis performs that gravitational mass is smaller for the polynomial profile P3 rather than the exponential profile P1. Very recently, Cromartie *et al.* [60] found in PSR J0740+6620 a super-massive NS with a mass about $M_{NS} = 2.14 \pm 0.10 M_{\odot}$, which renders strong constraint on the neutron star interior EoS. Therefore, we do require a stiff EoS which yields into greater maximum gravitational mass. It is obvious from Fig. 5 that the EoS is stiffer with inclusion of TNI contribution and the results of maximum gravitational mass is more in agreement with the observational data.

4 Summary and Conclusions

In the present paper, we investigate the effects of magnetic field on neutron stars properties. For this aim, we introduce three different magnetic field distributions and show how the magnetic field varies from the surface to the center of neutron stars.

In addition, we review different formalisms which define the effects of magnetic field on global properties of neutron stars. The magnetic field causes an anisotropy in pressure which breaks the spherical symmetry of the system and results in two-dimensional treatment. A comparison for magnetic neutron stars is carried out by solving the TOV equations (Adding the pure magnetic field contribution isotropically to the EoS) and the two-dimensional calculations (considering the magnetic pressure as perturbation). One can acquire that the corresponding gravitational mass calculated from the TOV solution is approximately larger than those of deformed solutions, while the equatorial radius obtained from the deformed

solutions is usually greater than the isotropic radius of TOV result. We should explain that if we use spherical metric to describe the structure of neutron stars, we will incorrectly gain stable stars with larger mass. On the other hand, when we follow the perturbed metric, only some of the field effects leads to an increase in the mass of the magnetars, while some of the magnetic pressure components generate the stellar deformation.

At last, the EoS and the structure of neutron stars is calculated by adding the contribution of TNI to AV_{18} two-body potential. This stiff EoS leads to more massive star which is in agreement with the recent observations.

Acknowledgment

We wish to thank University of Zanjan Research Councils.

References

[1] Duncan, R. C., & Thompson, C. 1992, ApJ, 392, L9

[2] Usov, V. V., 1992, Nature, 357, 472

[3] Spitler, L. G., & et.al. 2016, Nature, 531, 202

[4] Lai, D., & Shapiro, S. 1991, ApJ, 383, 745

[5] Tatsumi, T. 2000, Phys. Lett. B, 489, 280

[6] Kouveliotou, C., & et.al. 1998, Nature, 393, 235

[7] Olausen, S. A., & Kaspi, V. M. 2014, Astrophys. J. Suppl, 212, 6

[8] Chakrabarty, S., Bandyopadhyay, D., & Pal, S. 1997, Phys. Rev. Lett., 78, 2898

[9] Broderick, A., Prakash, M., & Lattimer, J. M. 2000, Astrophys. J., 537, 351

[10] Broderick, A., Prakash, M., & Lattimer, J. M. 2002, Phys. Lett., B, 531, 167

[11] Rabhi, A., Pais, H., Panda, P. K., & Providencia, C. 2009, J. Phys. G, 36, 115204

[12] Paulucci, L., Ferrer, E. J., de la Incera, V., & Horvath, J. E. 2011, Phys. Rev. D, 83, 043009

[13] Strickland, M., Dexheimer, V., & Menezes, D. P. 2012, Phys. Rev. D, 86, 125032

[14] Lopes, L. L.,& Menezes, D. P. 2012, Brazilian J. Phys., 42, 428

[15] Dexheimer, V., Menezes, D. P., & Strickland, M. 2014, J. Phys. G, 41, 015203

[16] Sinha, M., Huang, X. -G., & Sedrakian, A. 2013, Phys. Rev. D, 88, 025008

[17] Franzon, B., Dexheimer V., & Schramm, S. 2015, MNRAS, 456, 2937

[18] Gomes, R. O., Franzon, B., Dexheimer, V., & Schramm, S. 2017, ApJ, 850, 20

[19] Mao, G., Iwamoto, A., & Li, Z. 2003, Chin. J. Astron. Astrophys., 3, 359

[20] Sinha, M., Mukhopadhyay, M., & Sedrakian, A. 2013, Nucl. Phys. A, 898, 43

[21] Bandyopadhyay, D., Chakrabarty, S., & Pal, S. 1997, Phys. Rev. Lett., 79, 2176

[22] Lopes, L. L., & Menezes, D. P. 2015, JCAP, 08, 002

[23] Dexheimer, V., Negreiros, R., & Schramm, S., 2012, Eur. Phys. J. A, 48, 189

[24] Menezes, D. P., & Alloy, M. D. 2016, ArXiv e-prints, arXiv:1607.07687

[25] Dexheimer, V., Franzon, B., Gomes, R. O., Farias, R. L. S., & Avancini, S. S. 2017, Astronomische Nachrichten, 338, 1052

[26] Chatterjee, D., Novak, J., & Oertel, M. 2018, ArXiv e-prints, arXiv:1808.01778

[27] Chandrasekhar, S., & Fermi, E. 1953, ApJ, 118, 116

[28] Ferraro, V. C. A. 1954, ApJ, 119, 407

[29] Bonazzola, S., Gourgoulhon, E., Salgado, M., & Marck, J. A. 1993, A&A, 278, 421

[30] Bocquet, M., Bonazzola, S., Gourgoulhon, E., & Novak, J. 1995, A&A, 301, 757

[31] Cardall, C., Prakash, M., & Lattimer, J. M. 2001, ApJ, 554, 322

[32] Konno, K. 2001, A&A, 372, 594

[33] Yazadjiev, S. S. 2012, Phys. Rev. D, 85, 044030

[34] Kiuchi, K., & Yoshida, S. 2008, Phys. Rev. D, 78, 044045

[35] Frieben, J., & Rezzolla, L. 2012, MNRAS, 427, 3406

[36] Chatterjee, D., Elghozi, T., Novak, J., & Oertel, M. 2015, MNRAS, 447, 3785

[37] Konno, K., Obata, T.,& Kojima, Y. 1999, A&A, 352, 211

[38] Mallick, R., & Schramm, S. 2014, Phys. Rev. C, 89, 045805

[39] Manreza Paret, D., Horvath, J. E., & Perez Martnez, A. 2015, Res. Astron. Astrophys., 15, 975

[40] Zubairi, O., Romero, A., & Weber, F. 2015, J. Phys. Conf. Ser., 615, 012003

[41] Zubairi, O., & Weber, F. 2017, J. Phys. Conf. Ser., 845, 012005

[42] Bordbar, G. H., & Modarres, M. 1997, J. Phys. G: Nucl. Part. Phys., 23, 1631

[43] Lagaris, I. E., & Pandharipande, V. R. 1981, Nucl. Phys. A, 359, 349

[44] Shapiro, S. L., & Teukolsky, S. A. 1983, Black Holes, White Dwarfs, and Neutron Stars, Wiley, New York

[45] Hartle, J. B.,& Thorne, K. S. 1968, ApJ. 153, 807

[46] Hartle, J. B. 1973, Astrophys Space Sci., 24, 385

[47] Zamani, M., & Bigdeli, M. 2019, J. Phys. G: Nucl. Part. Phys., 46, 075201

[48] Isayev, A. A., & Yang, J. 2009, Phys. Rev. C, 80, 065801

[49] Isayev, A. A., & Yang, J. 2012, Phys. Lett. B, 707, 163

Table 1: The values of magnetic field in the surface and center of magnetars, associated with the sets of parameters used in this work. Global properties of neutron stars such as maximum gravitational mass, equatorial radius and deformation constant with different formalisms and different magnetic field profiles. The gravitational mass is given in solar mass ($M_\odot$).

		M1		M2			M3		
Magnetic field profile	$Log[B(G)]$	M	$R(km)$	M	$R_e(km)$	δ	M	$R_e(km)$	δ
$B=0$	-	1.71	8.40	-	-	-	-	-	-
P1 ($\beta=0.01,\gamma=3$)	$14.95-18.34$	1.80	8.92	1.75	8.91	0.89	1.75	9.47	0.83
P1 ($\beta=0.1,\gamma=1.5$)	$16.58-18.33$	1.81	9.32	1.73	9.27	0.83	1.75	9.42	0.83
P1 ($\beta=0.001,\gamma=5.1$)	$14.36-18.34$	1.84	9.21	1.75	9.22	0.84	1.76	9.74	0.79
P2 ($\gamma=1$)	$16.67-18.34$	1.74	8.65	1.73	8.74	0.93	1.73	8.94	0.90
P2 ($\gamma=3$)	$14.38-18.34$	1.72	8.40	1.71	8.49	0.99	1.72	8.60	0.96
P2 ($\gamma=5$)	$14.34-18.34$	1.71	8.39	1.71	8.49	0.99	1.71	8.54	0.97
P3 ($\beta=0.05,\gamma=1$)	$17.68-18.11$	1.72	8.77	1.71	8.89	0.87	1.73	9.44	0.70
P3 ($\beta=0.08,\gamma=1$)	$17.70-18.18$	1.74	9.39	1.71	9.49	0.81	1.73	9.75	0.64
P3 ($\beta=0.05,\gamma=1.2$)	$17.67-18.18$	1.73	8.82	1.71	8.91	0.86	1.73	9.50	0.70

[50] Aguirre, R., & Bauer, E. 2013, Phys. Lett. B, 721, 136

[51] Perez-Garcia, M. A. 2008, Phys. Rev. C, 77, 065806

[52] Perez-Garcia, M. A., & Navarro, J., Polls, A. 2009, Phys. Rev. C, 80, 025802

[53] Callen, H. B. 1960, Thermodynamics, Wiley, New York

[54] Clark, J. W., & Chao, N. C. 1969, Lett. Nuovo Cimento, 2, 185

[55] Modarres, M., Rajabi, A., & Moshfegh, H. R. 2007, Phys. Rev. C, 76, 064311

[56] Bordbar, G. H., & Modarres, M. 1998, Phys. Rev. C, 57, 714

[57] Bigdeli, M. 2012, Phys. Rev. C, 85, 034302

[58] Bigdeli, M. 2010, Phys. Rev. C, 82, 54312

[59] Asadi Aghbolaghi, Z., & Bigdeli, M. 2018, J. Phys. G: Nucl. Part. Phys., 45, 065101

[60] Cromartie, H. T., & et.al. 2019, ArXiv e-prints, arXiv:1904.06759

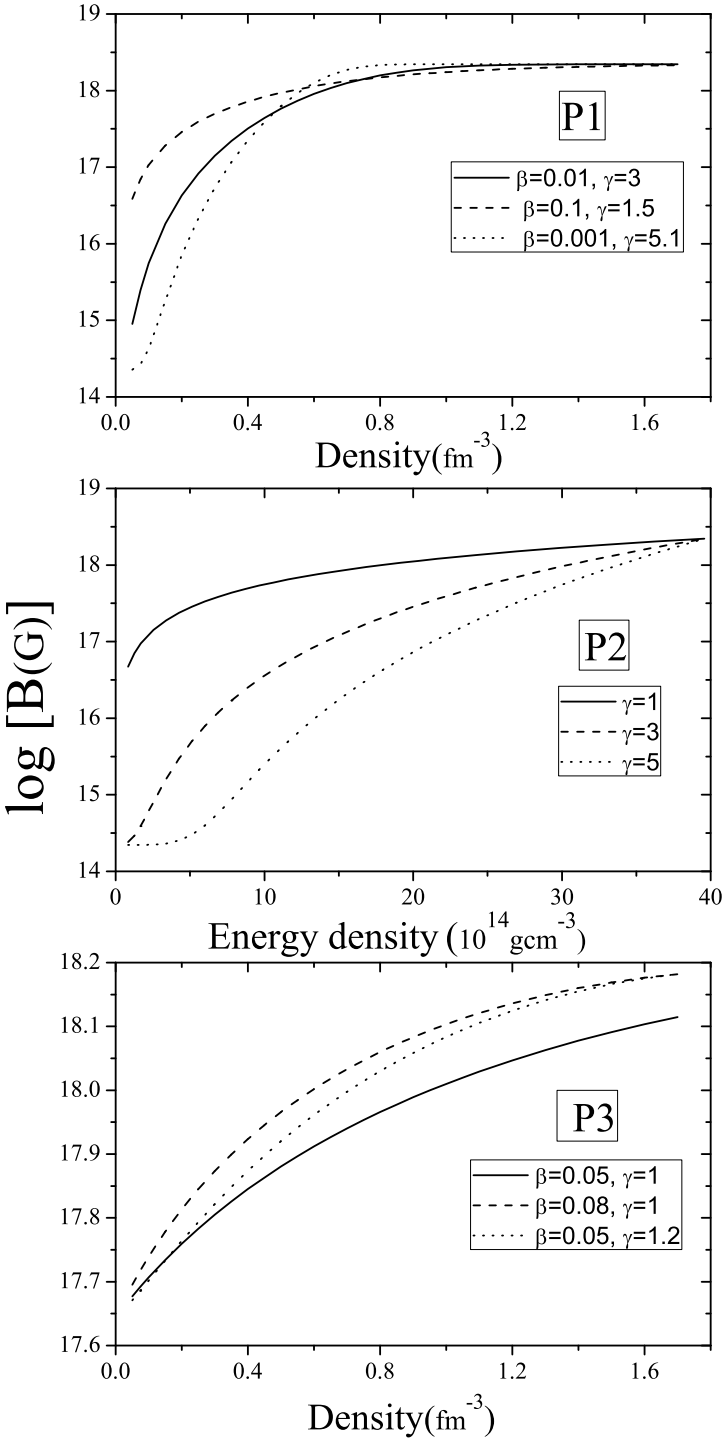

Figure 1: magnetic field profiles for different sets of β and γ.

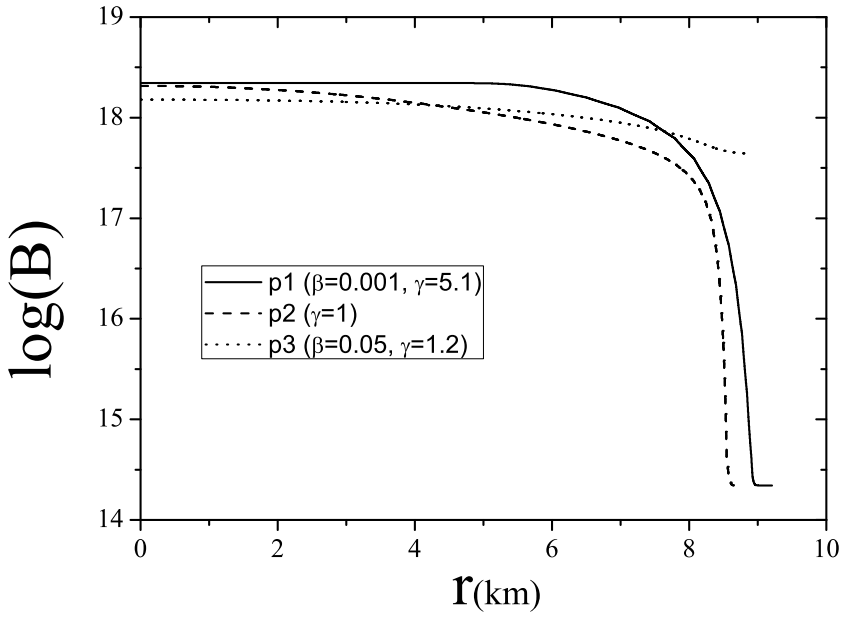

Figure 2: $\log(B)$ as a function of the stellar radius for different profiles. These results are obtained for the maximum mass configuration of the TOV solution.

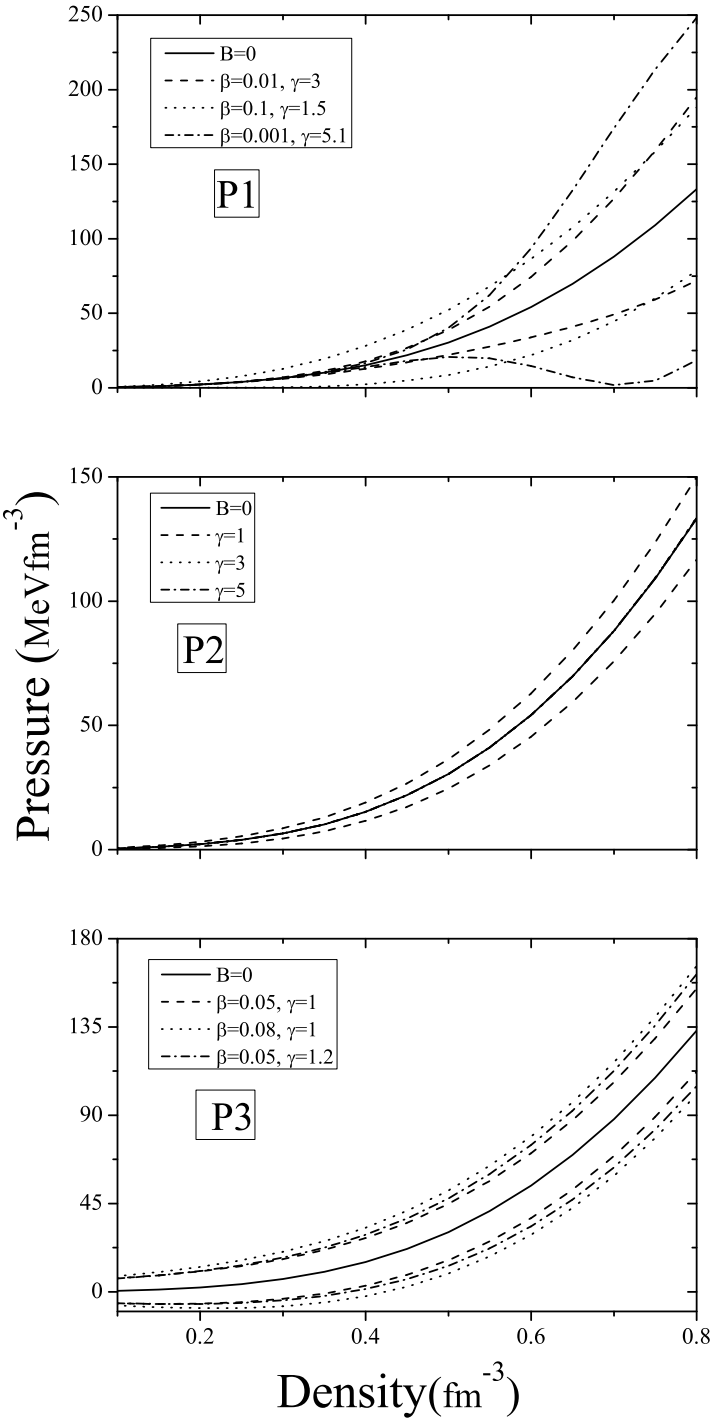

Figure 3: EoS of neutron matter for different sets of β and γ. The pressure of zero magnetic field is shown by filled line and the lines above this line are perpendicular pressure and the lines below this line are parallel pressures.

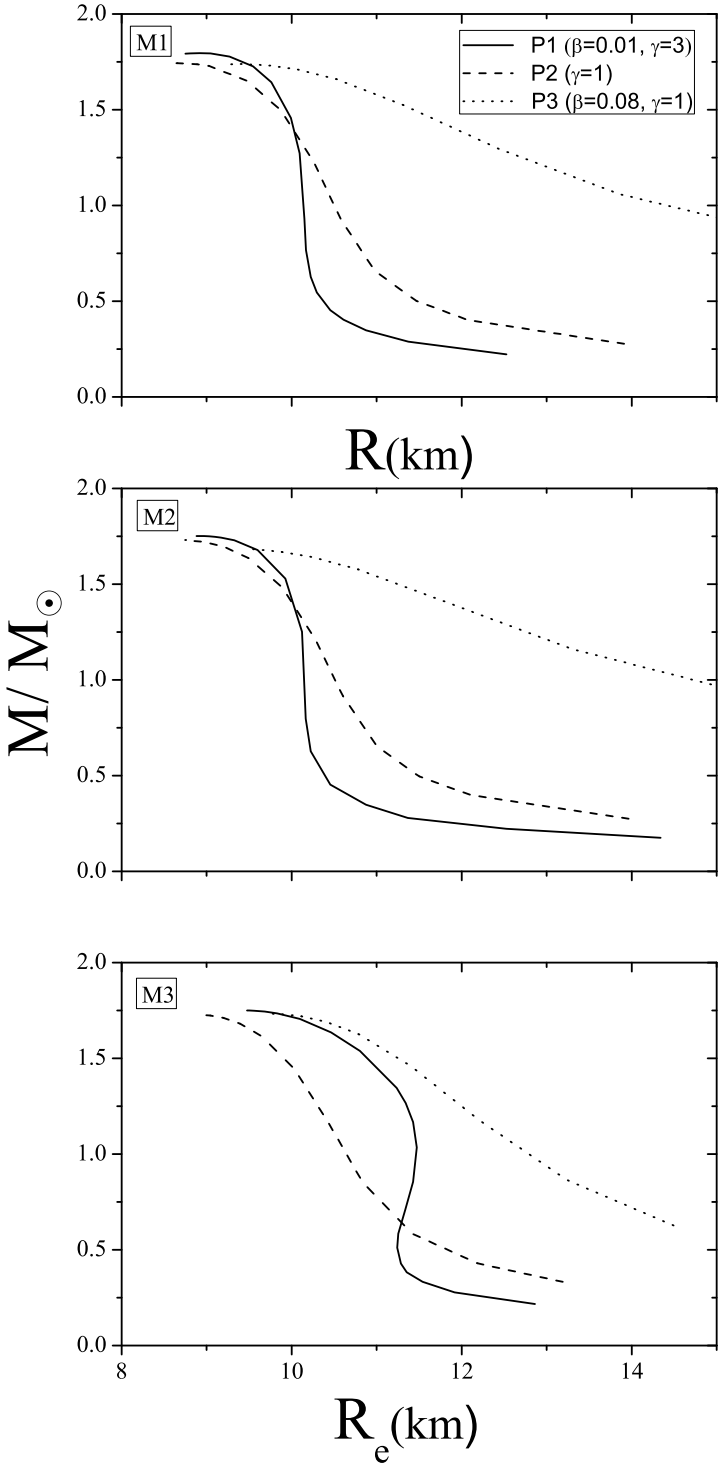

Figure 4: Mass-radius relations of magnetars for M1, M2 and M3 approaches and different field profiles.

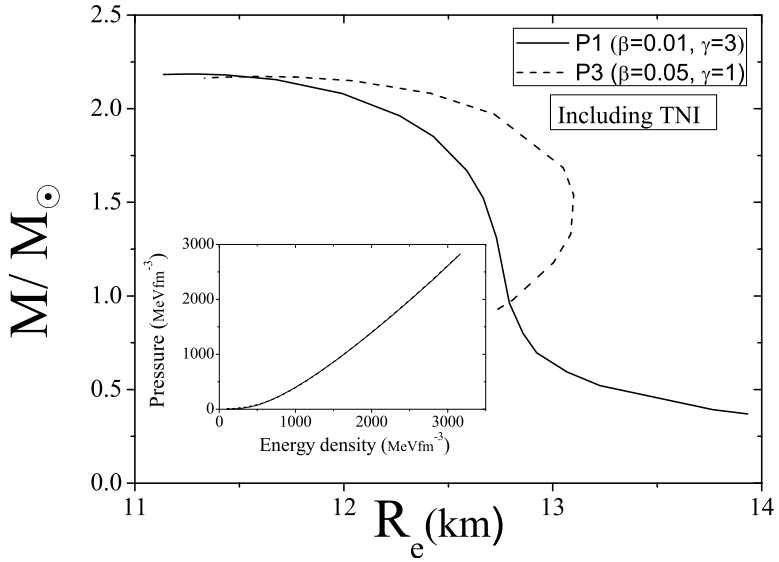

Figure 5: Mass-radius relations of magnetars for P1 and P3 field profiles and for M3 approach. The EoS of neutron matter is obtained by including TNI contribution. Results of EoS is merged in this panel.